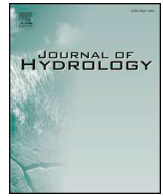




ELSEVIER

Contents lists available at ScienceDirect

Journal of Hydrology

journal homepage: www.elsevier.com/locate/jhydrol

Research papers

Centroidal Voronoi tessellation based methods for optimal rain gauge location prediction

Zichao (Wendy) Di^{a,*}, Viviana Maggioni^b, Yiwen Mei^b, Marilyn Vazquez^c, Paul Houser^d, Maria Emelianenko^e

^a Mathematics and Computer Science Division, Argonne National Laboratory, Lemont, IL, USA

^b Department of Civil, Environmental and Infrastructure Engineering, George Mason University, Fairfax, VA, USA

^c Mathematical Biosciences Institute, Ohio State University, Columbus, OH, USA

^d Department of Geography and Geoinformation Science, George Mason University, Fairfax, VA, USA

^e Department of Mathematical Sciences, George Mason University, Fairfax, VA, USA

ARTICLE INFO

This manuscript was handled by Marco Borga, Editor-in-Chief, with the assistance of Francesco Marra, Associate Editor

Keywords:

Rain gauges
CVT
Decorrelation
Optimal placement

ABSTRACT

We have used the following convention to highlight our changes in response to the referees' comments: red text indicates modification, blue text indicates addition, and margin parameters indicate responses to specific comment labeled as RxCy (Reviewer #x Comment #y) and RxMCy (Reviewer #x Minor Comment #y). With more satellite and model precipitation data becoming available, new analytical methods are needed that can take advantage of emerging data patterns to make well informed predictions in many hydrological applications. We propose a new strategy where we extract precipitation variability patterns and use correlation map to build the resulting density map that serves as an input to centroidal Voronoi tessellation construction that optimizes placement of precipitation gauges. We provide results of numerical experiments based on the data from the Alto-Adige region in Northern Italy and Oklahoma and compare them against actual gauge locations. This method provides an automated way for choosing new gauge locations and can be generalized to include physical constraints and to tackle other types of resource allocation problems.

1. Introduction

Precipitation is a critical variable in the water cycle, as it provides moisture for processes such as runoff, evapotranspiration, and groundwater recharge. Knowledge of the precipitation characteristics and patterns is therefore crucial for understanding land-climate interactions, for extreme event monitoring, and for water resource management. However, accurate precipitation information at fine space and time scales is difficult to obtain, as precipitation estimates from rain gauges, ground-based radars, satellite sensors, and numerical models are all affected by significant uncertainties, which can even be amplified when exposed to non-linear land surface model physics (Gottschalck et al., 2005; Hazra et al., 2019).

Rain gauge (or pluviometer) networks are the only direct method to measure precipitation and provide observations with high temporal resolution. As such, they are widely accepted as the benchmark for validating remotely-sensed precipitation products (e.g., Maggioni et al., 2016; Anagnostou et al., 2009). Point gauge measurements are often interpolated to obtain a spatially distributed rainfall field, whose

quality highly depends on the interpolation method used. Common interpolation methods include inverse-distance weighted averaging, ordinary kriging, and correlation length (Grieser, 2015), and more recent ones include co-kriging (Foehn et al., 2018) and methods that combine meteorological observations with regional climate model simulations (Wang et al., 2017).

However, obtaining a spatially representative precipitation field from rain gauges may require collecting a large number of observations at several locations to include different terrain, micro-climate, and vegetation variability. This translates into placing numerous gauges, which is costly in terms of maintenance and often not feasible because of location inaccessibility. Since rain gauges cannot offer spatially continuous information of precipitation (Kidd et al., 2012), it is desirable to place them in a strategic way, accounting for changes in spatio-temporal patterns and having a methodology that is able to adapt to climate instabilities as suggested in Emelianenko et al. (2019). This work proposes an automated method to identify the optimal locations of rain gauges in order to capture the spatial variability of precipitation systems in the region and therefore provide a spatially representative

* Corresponding author.

E-mail address: wendydi@mcs.anl.gov (Z.W. Di).

rain field. In comparison with kriging-based approaches (Wadoux et al., 2017; Pardo-Igúzquiza, 1998; Barca et al., 2008), our model enjoys a simpler analytical and numerical formulation owing to the natural minimization properties of the centroidal Voronoi tessellations (CVTs) described below, allowing to readily apply it to relatively large regions of interest.

Voronoi tessellations appear in many contexts and serve a variety of purposes. They are referred to as quantizations in the electrical engineering community (Agrell and Ericsson, 1998), as polygons of influence or Thiessen regions in geostatistics (Thiessen, 1911), as geodesic, icosahedral or hexagonal grids in climate system modeling (Ringler et al., 2000). The corresponding energy functional can be thought of as variation in statistical terminology, or as a cost functional in economic terms. The basic idea of this construction is to represent a large set of data by means of few representative points (i.e., generators).

While this general concept has been widely used in a variety of contexts, the special case of CVTs, which is used to denote Voronoi diagrams with the choice of generators that minimizes the energy functional, is less known due to the difficulties associated with its construction. This concept has been gaining popularity in the recent decades in many applications areas, ranging from biology and physics to finance, economics and social science (see Du et al., 2000; Chen and Xu, 2004; Ringler et al., 2008 and references therein). It is particularly well studied in the context of mesh generation, clustering, quantization, imaging, reduced order modeling and partial differential equations applications, where a number of theoretical results has been obtained attesting for its superior qualities comparing to other competing methodologies. To the best of our knowledge, applications of CVTs in hydrology so far have been limited to mesh generation (Lu et al., 2017) due to the flexibility provided by CVT for local mesh refinement.

The goal of this work is twofold. First, we want to introduce the concept of CVTs for precipitation pattern analysis and point out some recently developed numerical algorithms that help constructing CVTs in continuous and discrete settings. Second, we are applying the idea of CVTs in the context of optimal placement of rain gauges, similarly to how it was previously applied in finding optimal placement of schools, post offices, and other resources (Du et al., 1999). While other types of generalizations of the Voronoi construction have been explored, for instance, in the context of optimizing precipitation field using “similarity” of rainfall data at grid locations (e.g. using the Radar Polygon Method proposed in Cho et al. (2016)), this is the first application of the CVT methodology to modeling rainfall data and specifically to the optimization of rain gauge placement.

The practical aim of this study is to develop an automated strategy that would work for an arbitrary data in any geographical location. We draw attention to several modeling assumptions that are part of the algorithm presented herein and the implications of these assumptions on the algorithm performance based on several selected datasets.

We utilize the truncated-Newton (TN) method (Nash, 2000), which is a large-scale nonlinear optimization algorithm, to construct all CVT solutions. This method allows to considerably speed up the calculation comparing to techniques such as Lloyd method widely used in the engineering community (Lloyd, 1982), and has advantages over previously introduced modified Lloyd formulations, as shown in Di et al. (2012).

As in any CVT problem aimed at finding optimal placement of resources, one needs to have a local density estimator. When trying to optimize rain gauge placement, this density should be naturally related to the measure of local precipitation variability. In this work, we have used a variability estimator based on local covariance matrix computed at the decorrelation distance.

Overall, our aim in this work is to develop an automated strategy to optimally place rain gauge that could be employed in any geographical location in the future. To achieve this goal, we propose a CVT method that uses the local covariance matrix derived from local precipitation as the density estimator. This method could be applied to any

precipitation dataset, whether in situ, remotely sensed, or based on model simulations.

The article is organized as follows. Section 2 provides information on the CVT methodology and formulates the problem of optimal gauge placement, comparing to previously used approaches. Section 3 gives information on the data we used in this work. The proposed algorithm is presented in Section 4. We also demonstrate predictions given by this model with existing gauge locations in Section 5.

2. Methods

2.1. Voronoi and centroidal Voronoi tessellations

The idea of tessellating the region, i.e. decomposing the region into sub-regions, based on the locations of rain gauges has appeared in the early works of Thiessen (Thiessen, 1911).

The construction is simple. Consider a certain geographic region $W \subset \mathbb{R}^2$. Voronoi regions $\{V_i\}_{i=1}^k$ are generated by a set of points $\{\mathbf{x}_{ij}\}_{i=1}^k \in \mathbb{R}^2$ and are defined as follows:

$$V_i(\mathbf{x}_i) = \{\mathbf{x} \in W: \|\mathbf{x} - \mathbf{x}_i\| \leq \|\mathbf{x} - \mathbf{x}_j\|, j = 1, \dots, k; j \neq i\},$$

where $\|\cdot\|$ is any distance metric. In this work, we choose it to be the standard Euclidean norm. These regions cover the entire domain W and can be formed by drawing perpendicular bisectors to the segments joining consecutive generating points.

Given a certain desired “density” function $\rho(\mathbf{x})$, one can compute the tessellation error, i.e.

$$\mathcal{E}(\{\mathbf{x}_{ij}\}_{i=1}^k) = \min_{\{\mathbf{x}_{ij}\}_{i=1}^k} \sum_{i=1}^k \int_{V_i} \rho(\mathbf{x}) \|\mathbf{x} - \mathbf{x}_i\|^2 d\mathbf{x}. \quad (2.1)$$

It can be shown (Burkardt et al., 2006) that this happens precisely when $\mathbf{x}_i = \mathbf{x}_i^*$, where \mathbf{x}_i^* is the mass centroid of the corresponding Voronoi region V_i . A tessellation satisfying this property is called a “centroidal Voronoi tessellation”, or CVT for short. Notice that the above formulation may be extended to other more general cases, i.e. by considering other distance metrics $f(\|\cdot\|)$, other geometric constraints and periodic extensions (Du et al., 1999; Zhang et al., 2012).

The density function may be used to represent a variety of physical characteristics, such as local characteristic length-scale (Ringler et al., 2008), signal intensity (Emelianenko, 2010), desired grid resolution (Burkardt et al., 2006). In this work, we propose to use it for representing spatial rainfall variability, as described in Section 4. The classical method for constructing CVTs is the algorithm developed by Lloyd in the 1980s (Lloyd, 1982) which represents a fixed-point type iterative mechanism. More efficient methods for calculating CVTs have been developed in the past decades (Du and Emelianenko, 2006; Du and Emelianenko, 2008; Di et al., 2012). For an overview of CVT related numerical techniques we refer interested reader to (Du et al., 1999; Chen and Holst, 2011). To achieve a robust construction of CVT, we utilize TN to solve the resulting large-scale optimization problem due to its relative simplicity and robust performance comparing to other existing methods in terms of both accuracy and convergence speed (see the pseudocode given in Appendix B). We note that other methods might deliver comparable or better performance, possibly at the cost of an increase in numerical sophistication. Comparative study of numerical solvers suitable for this problem is outside the scope of the current work.

2.2. Problem formulation

There are several possible ways to formulate the problem of optimal placement of rain gauges in a certain region.

One method has been proposed in Okabe et al. (1992) and later used in Du et al. (1999). If k rain gauges locations in region $W \in \mathbb{R}^2$ are given by $\mathbf{x}_1, \dots, \mathbf{x}_k$ and $V_i \in W$ are the Voronoi region associated with the i -th

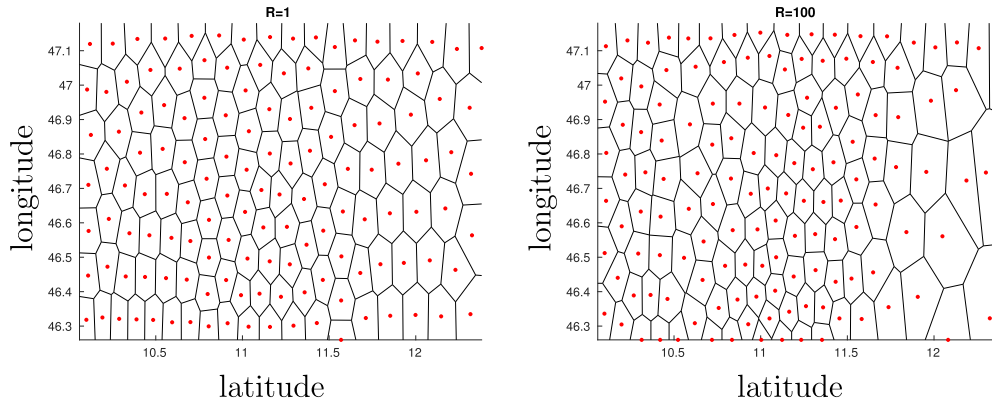


Fig. 1. Illustration of the effect of the ratio of R/r on the sizes of Voronoi regions. $r = 1$ is fixed for both figures.

gauge, one can minimize the expected squared approximation error for the amount of rainfall $z(\mathbf{x})$ treated as a random variable $z(\mathbf{x}) = m(\mathbf{x}) + \epsilon(\mathbf{x})$ with mean $m(\mathbf{x})$ and deviation $\epsilon(\mathbf{x})$. If the change in the average trend $m(\mathbf{x})$ is small compared with the variance $Var(\mathbf{x}) = E(\epsilon(\mathbf{x})^2) = \epsilon$, which is assumed to be constant, the expected squared approximation error can be approximated as

$$\mathcal{E}(\{\mathbf{x}_i\}_{i=1}^k) \approx \min_{\{\mathbf{x}_i\}_{i=1}^k} \sum_{i=1}^n \int_{V_i} 2\epsilon^2 [1 - Corr(\mathbf{x}, \mathbf{x}_i)] d\mathbf{x}, \tag{2.2}$$

where

$$Corr(\mathbf{x}, \mathbf{x}_i) = E[\epsilon(\mathbf{x})\epsilon(\mathbf{x}_i)] / [Var(\mathbf{x})Var(\mathbf{x}_i)] \tag{2.3}$$

is the (Pearson) linear correlation coefficient of the time series at locations \mathbf{x} and \mathbf{x}_i . Details on this derivation are given in Appendix A. Evaluation of (2.2) is computationally intensive, requiring calculation of pairwise correlations for all points inside the domain.

Notice that under the additional assumption that $Corr(\mathbf{x}, \mathbf{x}_i)$ only depends on the differences $\|\mathbf{x} - \mathbf{x}_i\|$, $\mathcal{E}(\{\mathbf{x}_i, V_i\}_{i=1}^k)$ can be thought of as a generalization of the CVT energy (2.1) given by:

$$\mathcal{E}(\{\mathbf{x}_i\}_{i=1}^k) = \sum_{i=1}^k \int_{V_i} \rho(\mathbf{x}) f(\|\mathbf{x} - \mathbf{x}_i\|) d\mathbf{x} \tag{2.4}$$

with distance metric $f(\|\mathbf{x} - \mathbf{x}_i\|) = 2\epsilon^2(1 - Corr(\mathbf{x}, \mathbf{x}_i))$ and $\rho(\mathbf{x}) = 1$. The combination of conditions of constant mean and variance together with $Corr(\mathbf{x}, \mathbf{x}_i) = Corr(\mathbf{x} - \mathbf{x}_i)$ is normally referred to as the *weak stationarity* assumption that might or might not hold in practice, as discussed for instance in Emelianenko et al. (2019). Effectively, in this formulation the distance plays the most important role, placing a small weight on highly correlated points and magnifying weakly correlated regions. The maximum value of the variance can be rather small depending on the data, which may possibly lead to slow convergence for commonly used numerical algorithms (Du et al., 2006).

In contrast with the above approach, standard CVT formulation (2.1) applied to the same problem allows achieving a similar effect by fixing Euclidean density and instead selecting appropriate density function ρ . This method is grounded on the observation that for the solutions to (2.1), the sizes of 2-dimensional Voronoi regions defined as $h_{V_i} = 2\max_{y \in V_i} \|\mathbf{x}_i - \mathbf{y}\|$ satisfy (Du et al., 1999):

$$\frac{h_{V_i}}{h_{V_j}} = \left(\frac{\rho(\mathbf{x}_i)}{\rho(\mathbf{x}_j)} \right)^{1/3}. \tag{2.5}$$

This is the approach advocated for in this work. One may rescale the density ρ to achieve any desired ratio of cell sizes based on a certain spatial distribution of interest, for instance, in Ringler et al. (2008), CVT mesh was generated using a velocity field. In this work we choose our density so that it satisfies the following conditions: $\sup_{\mathbf{x} \in W} \rho(\mathbf{x}) = \lim_{Corr(\mathbf{x}) \rightarrow C_{min}} \rho(\mathbf{x}) = R$ and $\inf_{\mathbf{x} \in W} \rho(\mathbf{x}) = \lim_{Corr(\mathbf{x}) \rightarrow C_{max}} \rho(\mathbf{x}) = r$. Here R and r are scale parameters and $Corr(\mathbf{x})$ denotes

effective (average) correlation at spatial location \mathbf{x} , with $-1 \leq C_{min} \leq Corr(\mathbf{x}) \leq C_{max} \leq 1, \forall \mathbf{x} \in W$. The method for computing this quantity based on averaging correlations at a “decorrelation” distance is discussed in 4.1. There are many functional forms such a relation can take. One choice is to consider power law relation of the type

$$\rho(\mathbf{x}) = r + R \left(\frac{C_{max} - Corr(\mathbf{x})}{C_{max} - C_{min}} \right)^\alpha, \tag{2.6}$$

where $\alpha > 0$ denotes the power exponent. The choice of this density has been motivated mainly by Ringler et al. (2008), but other choices might be argued for and will be explored in subsequent research.

This approach results in the following alternative formulation of the optimal rain gauge placement problem:

$$\min_{\{\mathbf{x}_i\}_{i=1}^k} \sum_{i=1}^k \int_{V_i} \left[r + R \left(\frac{C_{max} - Corr(\mathbf{x})}{C_{max} - C_{min}} \right)^\alpha \right] \|\mathbf{x} - \mathbf{x}_i\|^2 d\mathbf{x}. \tag{2.7}$$

The choice of parameters r, R, α is ultimately dependent on the data, the choice of the numerical optimization algorithm and particular application. Due to possible convergence issues, one needs to constrain density away from zero, so that $r > 0$. The scale parameter R magnifies the range of density values. Based on (2.5), the ratio R/r can be interpreted as an approximation for the ratio of largest and smallest Voronoi regions: $\frac{R}{r} \approx \frac{h_{max}}{h_{min}}$, and only affects Eqn. (2.7) linearly. We illustrate the role of this ratio in Fig. 1 by fixing $r = 1$ and varying R values. We defer to the values of $r = 10^{-6}$ and $R = 1$ in this work to provide the proof of concept. This choice gives a ratio of $R/r = 10^6$ and was optimized for the use of TN CVT construction algorithm.

Given desired region size ratio, parameter α allows to enhance the contrast between peaks and valleys of the function. It is expected that higher values of α will essentially penalize low correlation areas compared to high correlation (low density) areas, exaggerating density differences inside the given domain. The choice of the enhancement parameter α is described in details in Section 4.

3. Study regions and dataset

This work focused on two very different regions: Oklahoma in the United States and Alto-Adige in Northern Italy. The reason we chose these two domains is twofold. First, they are both covered by dense rain gauge networks that can be used as reference to evaluate the proposed algorithm. Second, they are characterized by different topography and therefore different precipitation processes.

Oklahoma is characterized by relatively uniform terrain, with gentle topography that rises from the southeastern corner to the tip of the panhandle. The continental climate of the region presents cold winters and hot summer seasons and a rainfall spatial pattern that exhibits a west-to-east (dry-to-wet) gradient. The study domain is covered by a dense network of meteorological stations, the Oklahoma Mesoscale

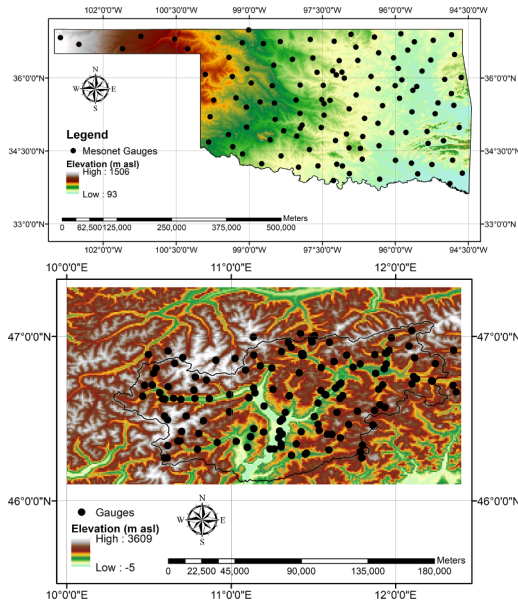


Fig. 2. Topographic maps with existing gauge locations: (top) Oklahoma region; (bottom) Adige region.

Network (hereinafter Mesonet; Brock et al., 1995), as seen in Fig. 2 (top). Although data collected at these stations were not used in this study, their locations were compared to the output from our proposed algorithm that optimizes gauge placement to fully capture the precipitation variability in the region.

A similar analysis was performed in Alto-Adige, located in the eastern Italian Alps. Unlike Oklahoma, this area is characterized by complex topography, with elevation ranging from 65 to almost 4000 m a.s.l.

Precipitation climatology in the area exhibits strong spatial gradients, with mean annual precipitation varying from ~ 500 mm in the Northwestern region to ~ 1700 mm in the Southeastern part (Maggioni et al., 2017; Nikolopoulos et al., 2015). A network of 192 rain gauges is available in the region. The rain gauges are distributed quite uniformly over the area (Fig. 2 (bottom)), providing a very dense gauge density ($\sim 1/70$ rain gauge/km²) for a mountainous area. For the regional studies across Oklahoma and Alto-Adige, we adopted a high resolution (1hour/0.04°) satellite precipitation product, the Precipitation Estimation from Remotely Sensed Information using Artificial Neural Networks (PERSIANN; Hsu et al., 1997; Sorooshian et al., 2000; Hsu et al., 2008), produced by the University of California, Irvine. The PERSIANN algorithm extracts and combines information from different types of data including Infra-Red (IR) brightness temperature images, rain gauges, and ground-based radar. Specifically, in this study we used the PERSIANN-Cloud Classification System (PERSIANN-CCS), which only applies information from IR observations from geostationary satellites with high sampling frequency (Hsu et al., 2010). The hourly PERSIANN-CCS was chosen among all available products because of its high spatial resolution (0.04). The PERSIANN-CCS algorithm follows four main steps: 1) separation of cloud images into cloud patches; 2) extraction of cloud features, including temperature, geometry, and texture; 3) clustering of cloud patches into organized subgroups; and 4) calibration of cloud-top brightness temperature and rainfall relationships for the identified subgroups using hourly gauge-corrected radar rainfall data (Hong et al., 2004). In the numerical examples below, we used a crude conversion of $0.04^\circ = 5$ [km] when presenting the results for both regions of interest. Improving this approximation or changing it for other geographic locations will bear no significant consequences in terms of the results.

4. Proposed algorithm

The main steps of the algorithm we are proposing are the following:

- Step 1 Build CVT density function based on the information on spatio-temporal correlations in a certain region using (2.6),
- Step 2 Solve the CVT minimization problem (2.7) to obtain optimal rain gauge locations for this region.

We are now going to discuss the details of Step 1, while an example of a TN-based CVT solver is provided in Appendix B. Note that other methods may be used in place of the TN method and might be equally effective depending on the properties of the data.

4.1. Effective correlation computation

Effective local correlation $Corr(\mathbf{x})$ is a key ingredient of the CVT density estimator used in our method. The approach we take is based on the calculation of local correlation of the time series at each grid point. The number of neighbors one should be taking into account in this computation is related to the decorrelation distance (radius), which is estimated using the exponential model with the so-called nugget effect (Ciach and Krajewski, 1999; Ciach and Krajewski, 2006):

$$\rho_g(d) = c_0 \exp \left[- \left(\frac{d}{d_0} \right)^{s_0} \right], \quad (4.8)$$

where d is the separation distance between two points, c_0 is the nugget parameter (which corresponds to the correlation value for the near-zero distances; Cressie, 1993), d_0 is the scale parameter (which corresponds to the spatial decorrelation distance), and s_0 is the correlogram shape parameter, which controls the behavior of the model near the origin for small separation distances. Note that $(1 - c_0)$ is the instant decorrelation due to random errors in the rainfall observations (Ciach, 2003).

We estimate $Corr(\mathbf{x})$ as the average of correlation coefficients between given point \mathbf{x} and locations on the circle $S(\mathbf{x}, d) = \{\mathbf{y} \in W : \|\mathbf{y} - \mathbf{x}\|_2 = d\}$ of radius d :

$$Corr(\mathbf{x}) = Corr_d(\mathbf{x}) = \frac{1}{|S(\mathbf{x}, d)|} \sum_{\mathbf{y} \in S(\mathbf{x}, d)} Corr(\mathbf{x}, \mathbf{y}), \quad (4.9)$$

where $Corr(\mathbf{x}, \mathbf{y})$ is the Pearson correlation coefficient given in (2.3).

Monte Carlo integration over the circle of radius d may be used to speed up the calculation of this quantity. Using uniform sampling $\mathbf{y}_1, \dots, \mathbf{y}_N$ over the region $\tilde{S}(\mathbf{x}, d) = \{\mathbf{y} \in W : d - 1 \leq \|\mathbf{y} - \mathbf{x}\|_2 \leq d + 1\}$, we define

$$Corr_N(\mathbf{x}) \approx \frac{1}{N} \sum_{i=1}^N Corr(\mathbf{x}, \mathbf{y}_i) \quad (4.10)$$

This method gives an error of the order of $O(1/\sqrt{N})$ (Caflich, 1998). The value of $N = 100$ was used in the numerical experiments described in Section 5. Importance sampling may be used to improve the accuracy of the Monte Carlo approximation of the local correlation map, but it was not explored in current work.

We define the separating distance d_0 at which the correlation is $1/e$ the correlation length for the (assumed) exponential variogram model:

$$d_0 = \min \left\{ d : Corr_d(\mathbf{x}) < \frac{1}{e} \right\} \quad (4.11)$$

Fig. 3 (left) demonstrates the calculation of the decorrelation distance for the case of the data collected over the Adige mountainous region in Northern Italy. We expect to have relatively small decorrelation distance over mountains, which is indeed true based on this data, from which a value of 9 grid points may be estimated, which corresponds to 45 [km]. Similar calculation performed over the flat region of Oklahoma shows decorrelation at 16 grid points, corresponding to 80 [km], as seen in Fig. 3 (right).

Now that the correlation component of the density is defined, we are ready to discuss a possible strategy for picking optimal value for α given expected number of rain gauges and a correlation threshold.

The choice of the density can be motivated by several factors,

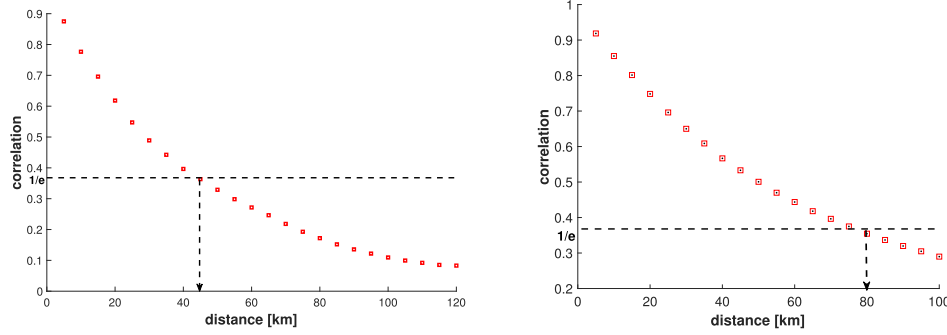


Fig. 3. Calculation of the decorrelation distance using $1/e$ -rule: (left) for the mountainous region in Northern Italy, with $d = 45$ [km]; (right) for the Oklahoma region, with $d = 80$ [km].

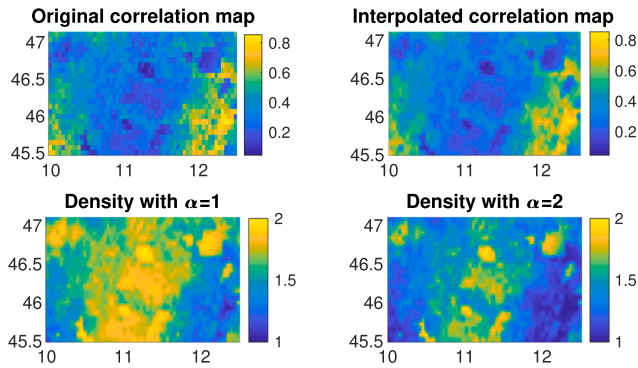


Fig. 4. Density computation for the Italy region: (top left) Effective correlation map based on the original data; (top right) interpolated map; (bottom left) density map constructed using (2.6) with $\alpha = 1$; (bottom right) density map for $\alpha = 2$.

including availability of resources and desired accuracy.

Fig. 4 shows CVT densities for Adige region, computed using formula (2.6) with $Corr(\mathbf{x})$ computed at the decorrelation distance as discussed above. Two different values of parameter α have been tested, resulting in clear differences in densities.

4.2. Optimal α and main algorithm

First, let us investigate the sensitivity of the density function given in (2.6) to the choice of α . We generate 50 densities based on different α evenly distributed between 0.5 and 25 (a subset of corresponding densities is shown in Fig. 6). Two error metrics (Wang et al., 2004) are used to quantify the differences between the two images (i.e., two different densities in this case): the root mean squared error (RMSE) and the structural similarity index (SSIM), which is used to resemble human perception. The closer the value of SSIM is to 1, the greater the similarity between two images. Fig. 5 shows the differences between densities for different α values and the first density, corresponding to $\alpha = 0.5$. As we can see from the consistent trend provided by different metrics, the change of density slows down dramatically as α increases. In view of these results, it is critical to carefully choose such parameter.

One may want to optimize the choice of parameter α based, for instance, on the desired number of rain gauges k_g to be placed in the regions with relative correlation below a certain threshold C_{tol} . Namely, we can pick density in such a way that we get approximately k_g locations with relative correlation below C_{tol} . We may choose an optimal value α^* as the smallest α satisfying

$$k = |\{\mathbf{x} | C_{rel}^\alpha = \left(\frac{Corr(\mathbf{x}) - C_{min}}{C_{max} - C_{min}} \right)^\alpha < C_{tol}\}| \leq k_g \quad (4.12)$$

where $|\cdot|$ denotes the number of grid points in the set.

If $\alpha = 1$ immediately satisfies condition (4.12), we stop. Otherwise

we keep increasing α until the desired resolution is obtained.

For instance, if the desired relative tolerance is $C_{tol} = 0.1$, meaning that locations with correlation below 10% are targeted, and if we are planning to place $k_g = 100$ gauges in a certain area, we will need to pick α to satisfy

$$k = |\{\mathbf{x} | C_{rel}^\alpha < 0.1\}| \leq 100$$

Fig. 6 gives a visualization of the optimal α selection procedure in the case of Adige data based on the above strategy, with the choice of $k_g = 60$, $C_{tol} = 0.1$ and default values $r = 1$, $R = 1$.

While the locations satisfying condition (4.12) are good candidates for initial gauge placement, this choice is not optimal in terms of the overall approximation of the precipitation in the region of interest. As discussed above, optimal placement is attained by computing CVT that minimizes the approximation error (2.1).

Finally, in Algorithm 1 we describe the main iterative algorithm for determining optimal placement for rain gauges for a given region.

Algorithm 1 Automatic selection of optimal gauge locations.

- 1: **procedure** GAUOPTIM
- 2: Define correlation threshold C_{tol} (default value $C_{tol} = 0.1$), desired number of gauges k_g .
- 3: Form the $N \times n$ observation matrix Y , where N and n denote the discrete spatial and temporal resolution, respectively.
- 4: Compute $Corr(\mathbf{y}_j)$ at each location \mathbf{y}_j , $j = 1, \dots, N$ using (4.10).
- 5: Compute decorrelation distance d using (4.11).
- 6: Interpolate the correlation map. Set $\alpha = 0$.
- 7: **loop:** Let $\alpha = \alpha + 1$.
- 8: Build the density map for the interpolated grid using (2.6).
- 9: **if** 4.12) is not satisfied **then**
- 10: **goto loop.**
- 11: **else**
- 12: Return optimal α .
- 13: Starting with k_g random points, find CVT-optimal generators \mathbf{x}_i , $i = 1, \dots, k_g$ using TN method given in Appendix B or any alternative method with the density (2.6).
- 14: Calculate CVT energy (2.1).

Apart from the precipitation time series data, the only input parameters needed to run the code are the correlation threshold C_{tol} and the number of gauges to be placed k_g . The default value for C_{tol} is 0.1, while the number of gauges can be arbitrary. If desired, the user may choose to construct the CVT tessellation for any given number of generators k_g starting immediately at line 13 of Algorithm 1.

5. Numerical results and discussion

Figs. 7 and 8 provide the results of applying Algorithm 1 to both regions and compare the optimal locations of rain gauges with existing rain gauge locations. The default values of $r = 10^{-6}$, $R = 1$ were chosen in all calculations.

As shown in Fig. 7, more gauges would be required where

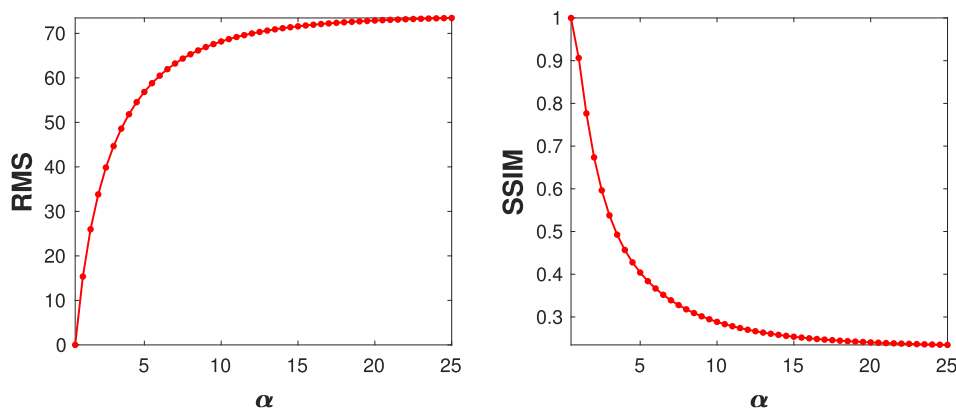


Fig. 5. Sensitivity of density formulation (2.6) to parameter α measured by RMS (left), and SSIM (right) error metrics in comparison to the density map with $\alpha_0 = 0.5$.

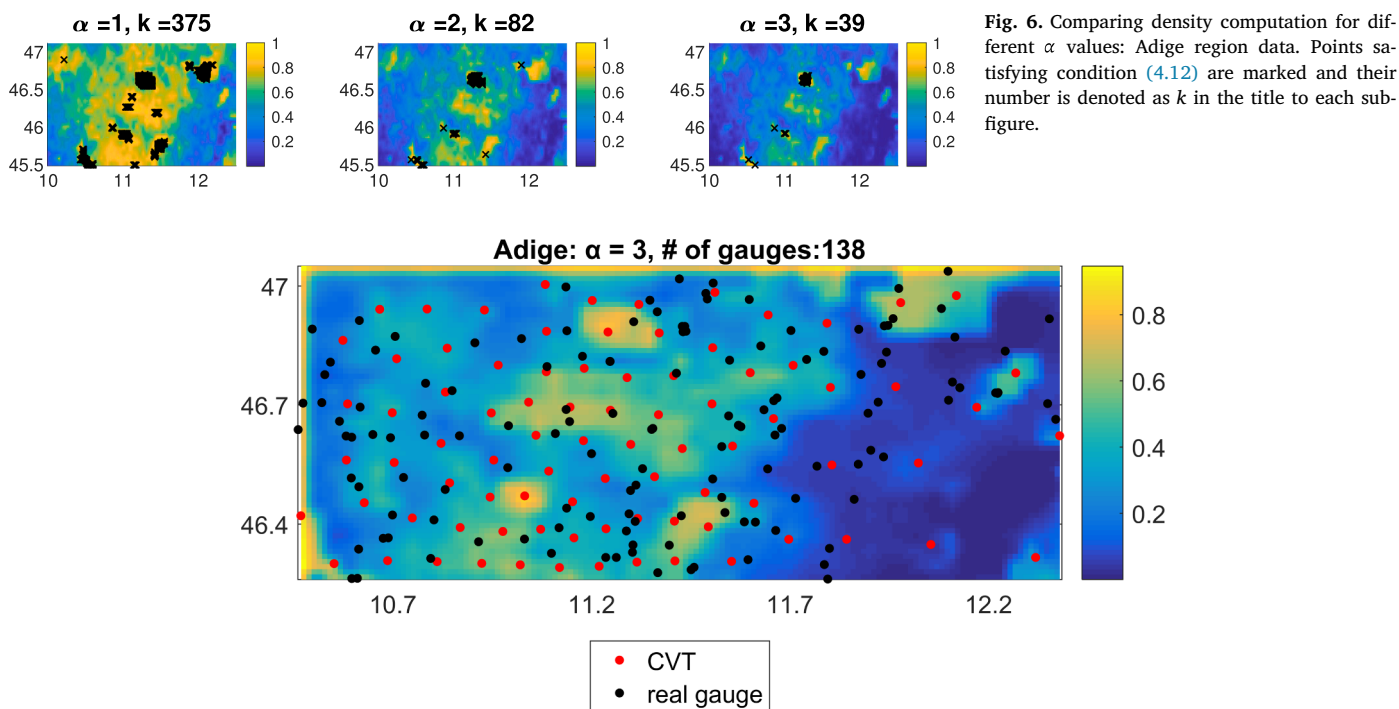


Fig. 7. Optimized rain gauge locations compared with real gauge data for the Adige dataset.

topography is the most complex, i.e., the northwestern region of Alto Adige, characterized by altitudes close to 4000 m a.s.l. On the other hand, in the valleys in the southeastern region, fewer gauges would be needed to fully capture the variability of precipitation. Similarly, in Oklahoma, where topography is more uniform than in Alto Adige, the gauge placement is also more homogeneous, with limited areas characterized by high density. This suggests that the proposed algorithm has the potential to optimize gauge placement based on observed precipitation patterns and variability that are partly linked to the geography of the region (e.g., orographic rainfall systems). In fact, elevation was shown in past literature to play a crucial role in rainfall variability (e.g., Sanchez-Moreno et al., 2014; Gebregiorgis and Hossain, 2012). Nevertheless, as topography is not the only variable affecting precipitation (e.g., Johnson and Hanson, 1995), future work should look at investigating gauge placement as a function of such information (e.g., climate, temperature, vegetation cover, etc.).

Since the output of the proposed framework is the optimal gauge locations provided above, one could wonder how different they are from the actual gauge locations in these regions. In other words, (1) can we identify actual gauges that are close to the optimal location and therefore fundamental to capture precipitation variability? and (2) can we identify gauges that are less important and, even if undergoing maintenance, would not be crucial to capture the full variability of the precipitation field in the area? In order to answer these questions, we look at Euclidean distance between a certain gauge and the closest optimal location for its simplicity and practical application, others can be considered, e.g., Ringler et al., 2008. We pick a measure of closeness as a circle of a certain radius and count the number of gauges that fall within that distance from any optimal location. Tables 1 and 2 give direct counts of the gauges that are close and far from optimal locations, and Figs. 9 and 10 provide visual representation of these results.

Obviously, some locations may be inaccessible (especially in

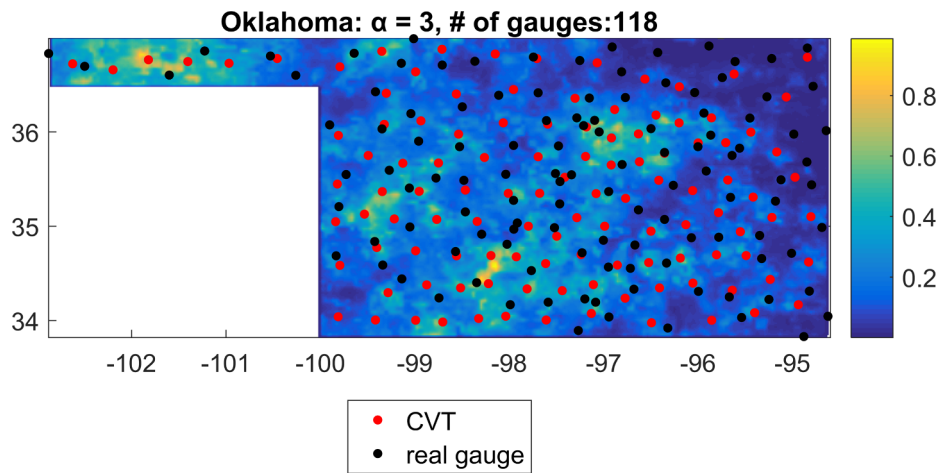


Fig. 8. Optimized rain gauge locations compared with real gauge data for the Oklahoma dataset.

Table 1

Adige region: number of gauges close to optimal locations for different closeness measures.

Radius (km)	Gauges within radius r	Gauges not within radius d
$r = 2$	8	130
$r = 5$	60	78
$r = 10$	132	6

Table 2

Oklahoma region: number of gauges close to optimal locations for different closeness measures

Radius (km)	Gauges within radius r	Gauges not within radius d
$r = 5$	7	111
$r = 10$	18	100
$r = 15$	49	69
$r = 15$	86	32

complex terrain) although optimal. The methodology introduced in this work can be modified to account for physical constraints and other resource allocation problems, but this is beyond the scope of this article and recommended for future work.

We now demonstrate the use of CVT energy as a way of measuring optimality of any given set of gauge locations and apply it to existing gauges in both regions. As shown in Fig. 11, the approximation error is significantly decreased by running the optimization routine. More specifically, the error decreases from 259.56 to 15.02 for Adige data and from $8.61 \cdot 10^4$ to $4.67 \cdot 10^4$ for Oklahoma, which are smaller than both from the real gauge locations. Since the goal of this work is to provide a

proof-of-concept of our CVT-based methodology, a systematic and rigorous validation process will be developed in the future.

6. Summary

We developed an automated strategy that allows to find optimal precipitation gauge locations in any given region based on the variability pattern in the precipitation over the region. The proposed algorithm could potentially be applied to any precipitation dataset (including re-analysis products) that is long enough to capture the temporal variability of precipitation, regardless of any seasonality. While variance was assumed to be stationary in this work, CVT framework allows to extend this approach to the non-stationary situation by keeping additional terms in the cost functional (8.13) and adjusting the corresponding density. We chose satellite-based observations because of their global (or quasi-global) coverage, making this method applicable anywhere else in the world. This is particularly useful when planning a field campaign to select sampling sites or when installing a new gauge network to pick the optimal number of gauges and their locations.

CRedit authorship contribution statement

Zichao (Wendy) Di: Conceptualization, Methodology, Writing - review & editing. **Viviana Maggioni:** Conceptualization, Data curation, Writing - review & editing. **Yiwen Mei:** Resources, Data curation, Visualization. **Marilyn Vazquez:** Writing - original draft. **Paul Houser:** Conceptualization. **Maria Emelianenko:** Conceptualization, Methodology, Writing - review & editing.

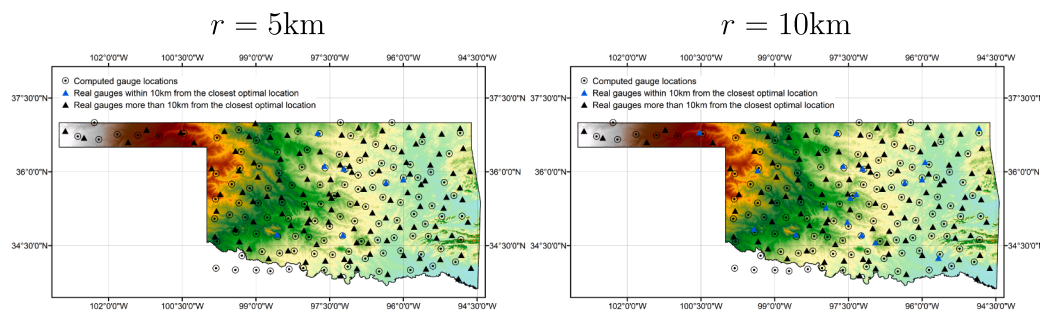


Fig. 9. Comparing existing locations with optimal placement for the Oklahoma region.

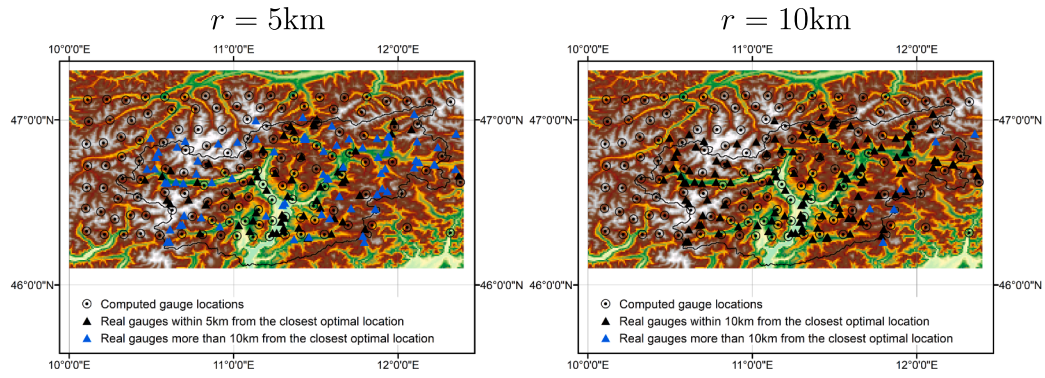


Fig. 10. Comparing existing locations with optimal placement for Adige region.

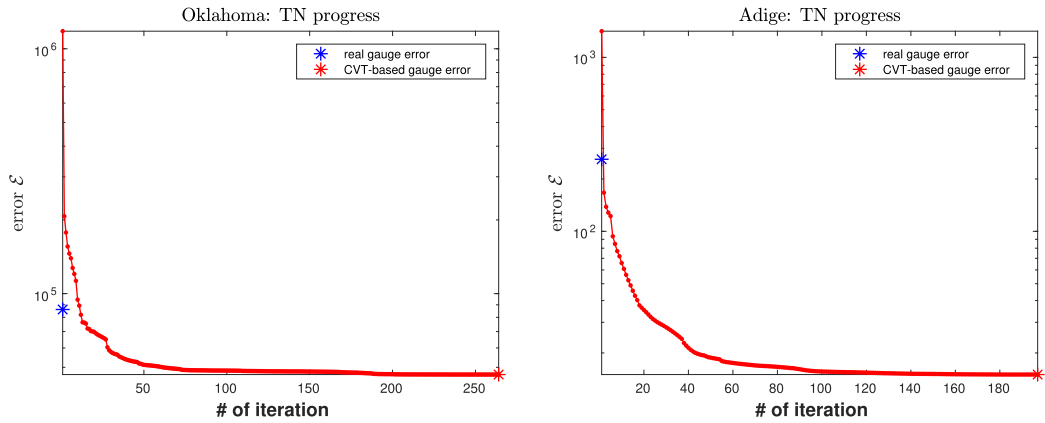


Fig. 11. Decay of the approximation error \mathcal{E} (2.1) during TN iteration for Oklahoma region (left) and Adige (right). CVT-based location denoted as a red asterisk gives a smaller error value comparing to the error computed for the real-gauge locations (shown as a blue asterisk).

Declaration of Competing Interest

The authors declare that they have no known competing financial interests or personal relationships that could have appeared to influence the work reported in this paper.

Acknowledgements

The authors are grateful to Ufficio Idrografico di Bolzano for providing Alto-Adige data. ME acknowledges support provided by the US National Science Foundation CAREER grant DMS-1056821 that funded Mason Modeling Days workshop where initial conceptualization of this work occurred.

Appendix A. Optimization problem formulation

Following (Okabe et al., 1992), let $z(\mathbf{x})$ be the random variable representing rainfall at location $\mathbf{x} \in W$. We can think of it as

$$z(\mathbf{x}) = m(\mathbf{x}) + \epsilon(\mathbf{x})$$

with $E(\epsilon(\mathbf{x})) = 0$, so that $m(\mathbf{x}) = E(z(\mathbf{x}))$ represents the average trend of the process over the given region.

Consider k rain gauges (pluviometers) $\mathbf{x}_1, \dots, \mathbf{x}_k$ placed within the region W and let V_i be the Voronoi region associated with the i -th gauge. As done by Thiessen back in 1911 (Thiessen, 1911), we can estimate the total precipitation in the region W as

$$Z = \int_S z(\mathbf{x})d\mathbf{x} = \sum_{i=1}^k \int_{V_i} z(\mathbf{x})d\mathbf{x} \approx \sum_{i=1}^n |V_i|z(\mathbf{x}_i)$$

This leads to the natural way to formulate the optimization problem for optimal gauge placement to minimize the expected squared approximation error:

$$\begin{aligned} \mathcal{E}(\mathbf{x}_1, \dots, \mathbf{x}_k) &= E\left[\sum_{i=1}^k \int_{V_i} (z(\mathbf{x}) - z(\mathbf{x}_i))^2 d\mathbf{x}\right] \\ &= \sum_{i=1}^k \int_{V_i} [(m(\mathbf{x}) - m(\mathbf{x}_i))]^2 + [Var(\mathbf{x}) - Var(\mathbf{x}_i)]^2 \\ &+ 2Var(\mathbf{x})Var(\mathbf{x}_i)[1 - Corr(\mathbf{x}, \mathbf{x}_i)]d\mathbf{x} \rightarrow \min \end{aligned} \tag{8.13}$$

Here $Var(\mathbf{x}) = E(\epsilon(\mathbf{x})^2)$ and $Var(\mathbf{x}_i) = E(\epsilon(\mathbf{x}_i)^2)$ denote variances at points \mathbf{x} and \mathbf{x}_i respectively and $Corr(\mathbf{x}, \mathbf{x}_i) = E[\epsilon(\mathbf{x})\epsilon(\mathbf{x}_i)]/[Var(\mathbf{x})Var(\mathbf{x}_i)]$ is the corresponding correlation of the time series at locations \mathbf{x} and \mathbf{x}_i .

If the variance $Var(\mathbf{x})$ is small compared to the change in the average trend $m(\mathbf{x})$:

$$\mathcal{E}(\mathbf{x}_1, \dots, \mathbf{x}_k) \approx \sum_{i=1}^k \int_{V_i} [(m(\mathbf{x}) - m(\mathbf{x}_i))]^2 d\mathbf{x} \rightarrow \min$$

One can solve this approximated problem to obtain optimal gauge placement in this case.

If on the other hand the change in the average trend $m(\mathbf{x})$ is small compared with the variance $Var(\mathbf{x})$, which is considered to be constant $Var(\mathbf{x}) = \epsilon$, the following approximation is valid:

$$\mathcal{E}(\mathbf{x}_1, \dots, \mathbf{x}_k) \approx \sum_{i=1}^k \int_{V_i} 2\epsilon^2 [1 - Corr(\mathbf{x}, \mathbf{x}_i)] d\mathbf{x} \rightarrow \min$$

Hence, if there is a relatively small change in the means, we can solve this approximated problem instead.

Notice that in this case $\mathcal{E}(\mathbf{x})$ is a variant of the CVT energy (2.4) with $f(\|\mathbf{x} - \mathbf{x}_i\|) = \epsilon^2(1 - Corr(\mathbf{x}, \mathbf{x}_i))$ and $\rho(\mathbf{x}) = 1$.

Appendix B. Truncated-Newton Algorithm for CVT calculation

Here, we give a brief review of the truncated Newton algorithm. For more details we refer readers to (Nash, 2000). To optimize a problem of the form

$$\min_{\mathbf{x}} f(\mathbf{x})$$

at the j -th TN iteration a search direction p is computed as an approximate solution to the Newton equations

$$\nabla^2 f(\mathbf{x}^{(j)})p = -\nabla f(\mathbf{x}^{(j)})$$

where $\mathbf{x}^{(j)}$ is the current approximation to the solution of the optimization problem. The search direction p is computed using the linear conjugate-gradient algorithm (CG). The necessary Hessian-vector products are estimated using finite differencing. The TN algorithm only requires that values of $f(\mathbf{x})$ and $\nabla f(\mathbf{x})$ are computed. TN has low storage requirements, and has low computational costs per iteration, and hence is suitable for solving large optimization problems (Nash and Nocedal, 1991).

The following are the steps necessary to compute discrete CVT using TN method using a pre-defined density function ρ :

- i. Given the discrete set of points $\mathbf{Y} = \{y_i\}_{i=1}^m \in W$,
- ii. Give the discrete energy function

$$\mathcal{G}(\mathbf{x}) = \sum_{V_i} \sum_j \rho(y_j) \|\mathbf{x}_i - y_j\|^2$$

where j is the index for those y included in the voronoi set V_i ,

- iii. Compute its corresponding gradient value

$$\nabla_i \mathcal{G}(\mathbf{x}) = \sum_j \rho(y_j) 2(\mathbf{x}_i - y_j),$$

- iv. By Taylor series:

$$\nabla \mathcal{G}(\mathbf{x} + \alpha v) = \nabla \mathcal{G}(\mathbf{x}) + \alpha \nabla^2 \mathcal{G}(\mathbf{x})v$$

we can approximate the necessary component $\nabla^2 \mathcal{G}(\mathbf{x})v$ of CG as $\nabla^2 \mathcal{G}(\mathbf{x})v = \frac{\nabla \mathcal{G}(\mathbf{x} + \alpha p) - \nabla \mathcal{G}(\mathbf{x})}{\alpha}$,

v. Substitute the above information to CG described as following to compute the search direction p :

- $r_0 := -\nabla \mathcal{G}(\mathbf{x})$
- $v_0 := r_0$
- $k := 0$
- repeat
 - $\alpha_k := \frac{r_k^T r_k}{v_k^T \nabla^2 \mathcal{G}(\mathbf{x})v_k}$
 - $p_{k+1} := p_k + \alpha_k v_k$
 - $r_{k+1} := r_k - \alpha_k \nabla^2 \mathcal{G}(\mathbf{x})v_k$
 - if r_{k+1} is sufficiently small then exit loop, end if
 - $\beta_k := \frac{r_{k+1}^T r_{k+1}}{r_k^T r_k}$
 - $v_{k+1} := r_{k+1} + \beta_k v_k$
 - $k := k + 1$
- end repeat

vi. Test whether $\nabla \mathcal{G}(\mathbf{x})p < 0$. If so, accept p as a descent direction, otherwise, take $p = -\nabla \mathcal{G}(\mathbf{x})$,

vii. Use Armijo line search to determine the step size α , then update \mathbf{x} by $\mathbf{x} = \mathbf{x} + \alpha p$,

viii. Go back to step iii) until a stopping criterion is reached.

The submitted manuscript has been created by UChicago Argonne, LLC, Operator of Argonne National Laboratory (“Argonne”). Argonne, a U.S. Department of Energy Office of Science laboratory, is operated under Contract No. DE-AC02-06CH11357. The U.S. Government retains for itself, and others acting on its behalf, a paid-up nonexclusive, irrevocable worldwide license in said article to reproduce, prepare derivative works, distribute copies to the public, and perform publicly and display publicly, by or on behalf of the Government. The Department of Energy will provide public access to these results of federally sponsored research in accordance with the DOE Public Access Plan. <http://energy.gov/downloads/doe-public-accessplan>

References

- Agrell, E., Ericsson, T., 1998. Optimization of lattices for quantization. *IEEE Trans. Inf. Theory* 44 (5), 1814–1828.
- Anagnostou, E., Maggioni, V., Nikolopoulos, E., Meskele, T., Hossain, F., Papadopoulos, A., 2009. Benchmarking high-resolution global satellite rainfall products to radar and rain-gauge rainfall estimates. *IEEE Trans. Geosci. Remote Sens.* 48 (4), 1667–1683.
- Barca, E., Passarella, G., Uricchio, V., 2008. Optimal extension of the rain gauge monitoring network of the Apulian Regional Consortium for Crop Protection. *Environ. Monitor. Assess.* 145 (1–3), 375–386.
- Brock, F., Crawford, K., Elliott, R., Cuperus, G., Stadler, S., Johnson, H., Eilts, M., 1995. The Oklahoma Mesonet: a technical overview. *J. Atmos. Oceanic Technol.* 12 (1), 5–19.
- Burkard, J., Gunzburger, M., Lee, H.-C., 2006. Centroidal Voronoi tessellation-based reduced order modeling of complex systems. *SIAM J. Sci. Comput.* 28 (2), 459–484.
- Caffisch, R.E., 1998. Monte Carlo and quasi-Monte Carlo methods. *Acta Numer.* 7, 1–49. <https://doi.org/10.1017/S096249290002804>.
- Chen, L., Holst, M., 2011. Efficient mesh optimization schemes based on optimal Delaunay triangulations. *Comp. Methods Appl. Mech. Eng.* 200, 967–984.
- Chen, L., Xu, J., 2004. Optimal Delaunay triangulations. *J. Comp. Math.* 22, 299–308.
- Cho, W., Lee, J., Park, J., Kim, D., 2016. Radar polygon method: an areal rainfall estimation based on radar rainfall imageries. *Stoch. Env. Res. Risk Assess.* 31, 275–289.
- Ciach, G., 2003. Local random errors in tipping-bucket rain gauge measurements. *J. Atmos. Oceanic Technol.* 20 (5), 752–759.
- Ciach, G., Krajewski, W., 1999. On the estimation of radar rainfall error variance. *Adv. Water Resour.* 22 (6), 585–595.
- Ciach, G., Krajewski, W., 2006. Analysis and modeling of spatial correlation structure in small-scale rainfall in Central Oklahoma. *Adv. Water Resour.* 29 (10), 1450–1463.
- Cressie, N., 1993. *Statistics for Spatial Data*. John Wiley and Sons.
- Di, Z., Emelianenko, M., Nash, S., 2012. Truncated Newton-based multigrid algorithm for centroidal Voronoi calculation. *Numer. Math. Theor. Meth. Appl.* 5 (1), 242–259.
- Du, Q., Emelianenko, M., 2006. Acceleration schemes for computing the centroidal Voronoi tessellations. *Numer. Linear Algebra Appl.* 13, 173–192.
- Du, Q., Emelianenko, M., 2008. Uniform convergence of a nonlinear energy-based multilevel quantization scheme via centroidal Voronoi tessellations. *SIAM J. Numer. Anal.* 46, 1483–1502.
- Du, Q., Faber, V., Gunzburger, M., 1999. Centroidal Voronoi tessellations: applications and algorithms. *SIAM Rev.* 41, 637–676.
- Du, Q., Gunzburger, M., Ju, L., 2000. Advances in studies and applications of centroidal Voronoi tessellations. *Numer. Math. Theor. Meth. Appl.* 3 (2), 119–142.
- Du, Q., Emelianenko, M., Ju, L., 2006. Convergence properties of the Lloyd algorithm for computing the centroidal Voronoi tessellations. *SIAM J. Numer. Anal.* 44, 102–119.
- Emelianenko, M., 2010. Fast multilevel CVT-based adaptive data visualization algorithm. *Numer. Math. Theor. Meth. Appl.* 3 (2), 195–211.
- Emelianenko, M., Maggioni, V., 2019. Mathematical challenges in measuring variability patterns for precipitation analysis. In: Kaper, H., Roberts, F. (Eds.), *Mathematics of Planet Earth*. Springer, pp. 49–61.
- Foehn, A., Hernández, J.G., Schaeffli, B., De Cesare, G., 2018. Spatial interpolation of precipitation from multiple rain gauge networks and weather radar data for operational applications in Alpine catchments. *J. Hydrol.* 563, 1092–1110.
- Gebregiorgis, A.S., Hossain, F., 2012. Understanding the dependence of satellite rainfall uncertainty on topography and climate for hydrologic model simulation. *IEEE Trans. Geosci. Remote Sens.* 51 (1), 704–718.
- Gottschalk, J., Meng, J., Rodell, M., Houser, P., 2005. Analysis of multiple precipitation products and preliminary assessment of their impact on global land data assimilation system land surface states. *J. Hydrometeorol.* 6, 573–598.
- Grieser, J., 2015. Interpolation of global monthly rain gauge observations for climate change analysis. *J. Appl. Meteorol. Climatol.* 54 (7), 1449–1464.
- Hazra, A., Maggioni, V., Houser, P., Antil, H., Noonan, M., 2019. A Monte Carlo-based multi-objective optimization approach to merge different precipitation estimates for land surface modeling. *J. Hydrol.* 570, 454–462.
- Hong, Y., Hsu, K.-L., Sorooshian, S., Gao, X., 2004. Precipitation estimation from remotely sensed imagery using an artificial neural network cloud classification system. *J. Appl. Meteorol.* 43 (12), 1834–1853.
- Hsu, K.-L., Sorooshian, S., 2008. Satellite-based precipitation measurement using PERSIANN system. In: *Hydrol. Model. Water Cycle*. Springer-Verlag, Berlin, Germany, pp. 27–48.
- Hsu, K.-L., Gao, X., Sorooshian, S., Gupta, H.V., 1997. Precipitation estimation from remotely sensed information using artificial neural networks. *J. Appl. Meteorol.* 36 (9), 1176–1190.
- Hsu, K.-L., Behrangi, A., Iman, B., Sorooshian, S., 2010. Extreme precipitation estimation using satellite-based PERSIANN-CCS algorithm. In: Gebremichael, M., Hossain, F. (Eds.), *Satellite Rainfall Applications for Surface Hydrology*. Springer, pp. 49–67.
- Johnson, G., Hanson, C., 1995. Topographic and atmospheric influences on precipitation variability over a mountainous watershed. *J. Appl. Meteorol.* 34 (1), 68–87.
- Kidd, C., Bauer, P., Turk, J., Huffman, G., Joyce, R., Hsu, K., Braithwaite, D., 2012. Intercomparison of high-resolution precipitation products over northwest Europe. *J. Hydrometeorol.* 13 (6783).
- Lloyd, S., 1982. Least square quantization in PCM. *IEEE Trans. Inf. Theory* 28, 129–137.
- Lu, J., Sakaguchi, K., Yang, Q., Leung, L.R., Chen, G., Zhao, C., Swenson, E., Hou, Z.J., 2017. Examining the hydrological variations in an aquaplanet world using wave activity transformation. *J. Clim.* 30 (7), 2559–2576.
- Maggioni, V., Meyers, P., Robinson, M., 2016. A review of merged high-resolution satellite precipitation product accuracy during the tropical rainfall measuring mission (TRMM) era. *J. Hydrometeorol.* 17 (4), 1101–1117.
- Maggioni, V., Nikolopoulos, E., Anagnostou, E., Borga, M., 2017. Modeling satellite precipitation errors over mountainous terrain: the influence of gauge density, seasonality, and temporal resolution. *IEEE Trans. Geosci. Remote Sens.* 55 (7), 4130–4140.
- Nash, S.G., 2000. A survey of truncated-Newton methods. *J. Comput. Appl. Math.* 124 (1), 45–59.
- Nash, S.G., Nocedal, J., 1991. A numerical study of the limited memory BFGS method and the truncated-Newton method for large scale optimization. *SIOPT* 1, 358–372.
- Nikolopoulos, E.I., Borga, M., Marra, F., Crema, S., Marchi, L., 2015. Debris flows in the eastern Italian Alps: seasonality and atmospheric circulation patterns. *Natural Hazards Earth Syst. Sci.* 15 (3), 647–656.
- Okabe, A., Boots, B., Sugihara, K., 1992. *Spatial Tessellations; Concepts and Applications of Voronoi Diagrams*. Wiley, Chichester.
- Pardo-Igúzquiza, E., 1998. Optimal selection of number and location of rainfall gauges for areal rainfall estimation using geostatistics and simulated annealing. *J. Hydrol.* 210 (1–4), 206–220.
- Ringler, T., Heikes, R., Randall, D., 2000. Modeling the atmospheric general circulation using a spherical geodesic grid: a new class of dynamical cores. *Mon. Weather Rev.* 128, 2471–2490.
- Ringler, T., Ju, L., Gunzburger, M., 2008. A multiresolution method for climate system modeling: application of spherical centroidal Voronoi tessellations. *Ocean Dyn.* 58, 475–498.
- Sanchez-Moreno, J., Mannaerts, C., Jetten, V., 2014. Influence of topography on rainfall variability in Santiago island, cape verde. *Int. J. Climatol.* 34 (4), 1081–1097.
- Sorooshian, S., Hsu, K.-L., Gao, X., Gupta, H.V., Imam, B., Braithwaite, D., 2000. Evaluation of PERSIANN system satellite-based estimates of tropical rainfall. *Bull. Am. Meteorol. Soc.* 81, 2035–2046.
- Thiessen, A., 1911. Precipitation averages for large areas. *Mon. Weather Rev.* 39, 1081–1084.
- Wadoux, A.-C., Brus, D., Rico-Ramirez, M., Heuvelink, G., 2017. Sampling design optimisation for rainfall prediction using a non-stationary geostatistical model. *Adv. Water Resour.* 107, 126–138.
- Wang, Z., Bovik, A.C., Sheikh, H.R., Simoncelli, E.P., et al., 2004. Image quality assessment: from error visibility to structural similarity. *IEEE Trans. Image Process.* 13 (4), 600–612.
- Wang, Y., Yang, H., Yang, D., Qin, Y., Gao, B., Cong, Z., 2017. Spatial interpolation of daily precipitation in a high mountainous watershed based on gauge observations and a regional climate model simulation. *J. Hydrometeorol.* 18 (3), 845–862.
- Zhang, J., Emelianenko, M., Du, Q., 2012. Periodic centroidal Voronoi tessellations. *Int. J. Numer. Anal. Model.* 9, 950–969.